



HAL
open science

Singular Curves in the Joint Space and Cusp Points of 3-RPR parallel manipulators

Mazen Zein, Philippe Wenger, Damien Chablat

► **To cite this version:**

Mazen Zein, Philippe Wenger, Damien Chablat. Singular Curves in the Joint Space and Cusp Points of 3-RPR parallel manipulators. *Robotica*, 2007, 25 (6), pp.717-724. 10.1017/S0263574707003785 . hal-00184991

HAL Id: hal-00184991

<https://hal.science/hal-00184991v1>

Submitted on 4 Nov 2007

HAL is a multi-disciplinary open access archive for the deposit and dissemination of scientific research documents, whether they are published or not. The documents may come from teaching and research institutions in France or abroad, or from public or private research centers.

L'archive ouverte pluridisciplinaire **HAL**, est destinée au dépôt et à la diffusion de documents scientifiques de niveau recherche, publiés ou non, émanant des établissements d'enseignement et de recherche français ou étrangers, des laboratoires publics ou privés.

SINGULAR CURVES IN THE JOINT SPACE AND CUSP POINTS OF 3-*RPR* PARALLEL MANIPULATORS

Mazen ZEIN, Philippe Wenger and Damien Chablat

Institut de Recherche en Communications et Cybernétique de Nantes UMR CNRS 6597

1, rue de la Noë, BP 92101, 44312 Nantes Cedex 03 France

E-mail address: Mazen.Zein@irccyn.ec-nantes.fr

Phone: 0033240376955

Fax: 0033240376930

Abstract

*This paper investigates the singular curves in the joint space of a family of planar parallel manipulators. It focuses on special points, referred to as cusp points, which may appear on these curves. Cusp points play an important role in the kinematic behavior of parallel manipulators since they make possible a nonsingular change of assembly mode. The purpose of this study is twofold. First, it exposes a method to compute joint space singular curves of 3-*RPR* planar parallel manipulators. Second, it presents an algorithm for detecting and computing all cusp points in the joint space of these same manipulators.*

1. Introduction

Because at a singularity a parallel manipulator loses its stiffness, it is of primary importance to be able to characterize these special configurations. This is, however, a very challenging task for a general parallel manipulator¹. Planar parallel manipulators have received a lot of attention¹⁻⁸ because of their relative simplicity with respect to their spatial counterparts. Moreover, studying the former may help understand the latter. Planar manipulators with three extensible leg rods, referred to as 3-*RPR* manipulators, have often been studied. Such manipulators may have up to six assembly modes⁷. The direct kinematics can be written in a polynomial of degree six³. Moreover, as is the case in most parallel manipulators, the singularities coincide with the set of configurations where two direct kinematic solutions coincide. It was first pointed out that to move from one assembly

mode to another, the manipulator should cross a singularity⁷. However, Innocenti⁸ showed, using numerical experiments, that this statement is not true in general. More precisely, this statement is only true under some special geometric conditions, such as similar base and mobile platforms^{9,10}. In fact, an analogous phenomenon exists in serial manipulators that can change their posture (inverse kinematic solution) without meeting a singularity in general, but not under special geometric simplifications^{8,11-13}. The nonsingular change of posture in serial manipulators was shown to be associated with the existence of points in the workspace where three inverse kinematic solutions meet, called cusp points¹³. Cusp points in serial manipulators were determined by looking for the triple roots of the inverse kinematics polynomial¹³ or from the equation of the workspace boundary¹⁴. Likewise, McAree⁹ pointed out that for a 3-*RPR* parallel manipulator (as well as for its spatial counterpart, the octahedral manipulator), if a point with triple direct kinematic solutions exists in the joint space, then the nonsingular change of assembly mode is possible. A condition for three direct kinematic solutions to coincide was established. However, no systematic exploitation of this condition was possible because the algebra involved was too complicated and to the authors' knowledge, the work of McAree⁹ has never been pursued yet. Wenger¹⁵ showed that to accomplish a non-singular assembly-mode changing motion, a 3-*RPR* manipulator platform should encircle a cusp point in its joint space. Thus, determination of cusp points is of interest for planning trajectories. A procedure for computing joint space singularities of 3-*RPR* parallel manipulators was established in a previous paper¹⁶, where the cusp points were shown on the joint space singularities of these manipulators but no solution was proposed for computing these cusp points.

In this paper, the abovementioned condition for computing cusp points is reviewed and exploited. An algorithm for the systematic detection of cusp points is developed. The method¹⁶ for computing and representing joint space singularities of 3-*RPR* planar parallel manipulators is first recalled. A descriptive analysis of the singular curves in slices of the joint space of 3-*RPR* parallel manipulators is conducted. It is shown that the number of cusp points depends on the slice of the

2.2 Constraint equations

Let $\mathbf{L} \equiv (\rho_1, \rho_2, \rho_3)$ define the lengths of the three leg rods and let $\boldsymbol{\theta} \equiv (\theta_1, \theta_2, \theta_3)$ define the three angles between the leg rods and the x -axis. The six parameters $(\mathbf{L}, \boldsymbol{\theta})$ can be regarded as a configuration of the manipulator but only three of them are independent, so that the configuration space is a 3-dimensional manifold embedded in a 6-dimensional space. The dependency between $(\mathbf{L}, \boldsymbol{\theta})$ can be identified by writing the fixed distances between the three vertices of the mobile platform B_1, B_2, B_3 :

$$\begin{cases} \Gamma_1(\mathbf{L}, \boldsymbol{\theta}) = [\mathbf{b}_2(\mathbf{L}, \boldsymbol{\theta}) - \mathbf{b}_1(\mathbf{L}, \boldsymbol{\theta})]^T [\mathbf{b}_2(\mathbf{L}, \boldsymbol{\theta}) - \mathbf{b}_1(\mathbf{L}, \boldsymbol{\theta})] - d_1^2 = 0 \\ \Gamma_2(\mathbf{L}, \boldsymbol{\theta}) = [\mathbf{b}_3(\mathbf{L}, \boldsymbol{\theta}) - \mathbf{b}_2(\mathbf{L}, \boldsymbol{\theta})]^T [\mathbf{b}_3(\mathbf{L}, \boldsymbol{\theta}) - \mathbf{b}_2(\mathbf{L}, \boldsymbol{\theta})] - d_2^2 = 0 \\ \Gamma_3(\mathbf{L}, \boldsymbol{\theta}) = [\mathbf{b}_1(\mathbf{L}, \boldsymbol{\theta}) - \mathbf{b}_3(\mathbf{L}, \boldsymbol{\theta})]^T [\mathbf{b}_1(\mathbf{L}, \boldsymbol{\theta}) - \mathbf{b}_3(\mathbf{L}, \boldsymbol{\theta})] - d_3^2 = 0 \end{cases} \quad (1)$$

where \mathbf{b}_i is the vector defining the coordinates of B_i in the reference frame as function of \mathbf{L} and $\boldsymbol{\theta}$. For more simplicity, $(\mathbf{L}, \boldsymbol{\theta})$ will be omitted in the following equations.

Expanding each Γ_i as a series about the configuration $(\mathbf{L}, \boldsymbol{\theta})$ yields

$$\begin{aligned} \Delta\Gamma_i &= \left(\sum_{j=1}^3 \Delta\theta_j \frac{\partial}{\partial\theta_j} + \sum_{j=1}^3 \Delta\rho_j \frac{\partial}{\partial\rho_j} \right) \Gamma_i + \frac{1}{2!} \left(\sum_{j=1}^3 \Delta\theta_j \frac{\partial}{\partial\theta_j} + \sum_{j=1}^3 \Delta\rho_j \frac{\partial}{\partial\rho_j} \right)^2 \Gamma_i + \dots + \\ &\frac{1}{n!} \left(\sum_{j=1}^3 \Delta\theta_j \frac{\partial}{\partial\theta_j} + \sum_{j=1}^3 \Delta\rho_j \frac{\partial}{\partial\rho_j} \right)^n \Gamma_i + \dots = 0 \end{aligned} \quad (2)$$

If one keeps only the first-order and second-order terms, Eq.(2) can be written in matrix form as follows:

$$\Delta\Gamma = \frac{\partial\Gamma}{\partial\boldsymbol{\theta}} \Delta\boldsymbol{\theta} + \frac{\partial\Gamma}{\partial\mathbf{L}} \Delta\mathbf{L} + \frac{1}{2} \begin{bmatrix} \Delta\boldsymbol{\theta}^T \frac{\partial^2\Gamma_1}{\partial\boldsymbol{\theta}^2} \Delta\boldsymbol{\theta} \\ \Delta\boldsymbol{\theta}^T \frac{\partial^2\Gamma_2}{\partial\boldsymbol{\theta}^2} \Delta\boldsymbol{\theta} \\ \Delta\boldsymbol{\theta}^T \frac{\partial^2\Gamma_3}{\partial\boldsymbol{\theta}^2} \Delta\boldsymbol{\theta} \end{bmatrix} + \begin{bmatrix} \Delta\boldsymbol{\theta}^T \frac{\partial^2\Gamma_1}{\partial\boldsymbol{\theta}\partial\mathbf{L}} \Delta\mathbf{L} \\ \Delta\boldsymbol{\theta}^T \frac{\partial^2\Gamma_2}{\partial\boldsymbol{\theta}\partial\mathbf{L}} \Delta\mathbf{L} \\ \Delta\boldsymbol{\theta}^T \frac{\partial^2\Gamma_3}{\partial\boldsymbol{\theta}\partial\mathbf{L}} \Delta\mathbf{L} \end{bmatrix} + \frac{1}{2} \begin{bmatrix} \Delta\mathbf{L}^T \frac{\partial^2\Gamma_1}{\partial\mathbf{L}^2} \Delta\mathbf{L} \\ \Delta\mathbf{L}^T \frac{\partial^2\Gamma_2}{\partial\mathbf{L}^2} \Delta\mathbf{L} \\ \Delta\mathbf{L}^T \frac{\partial^2\Gamma_3}{\partial\mathbf{L}^2} \Delta\mathbf{L} \end{bmatrix} = 0 \quad (3)$$

Equation (3) can be used to describe an arbitrary local motion at a given configuration of the manipulator⁹. When first order terms of Eq.(3) are sufficient to describe the motion, the manipulator

is in a regular configuration and the following equation (4) can be used instead of Eq.(3):

$$\frac{\partial \Gamma(\mathbf{L}, \boldsymbol{\theta})}{\partial \boldsymbol{\theta}} \Delta \boldsymbol{\theta} + \frac{\partial \Gamma(\mathbf{L}, \boldsymbol{\theta})}{\partial \mathbf{L}} \Delta \mathbf{L} = 0 \quad (4)$$

Otherwise the configuration $(\mathbf{L}, \boldsymbol{\theta})$ is special and the manipulator meets a singularity. This happens when the constraint Jacobian $\partial \Gamma / \partial \boldsymbol{\theta}$ drops rank so that the second order terms of equation (3) are required to describe the constraints. The three vertices of the moving platform have the following coordinates in the fixed reference frame,

$$\mathbf{b}_1 = [\rho_1 \cos(\theta_1) \quad \rho_1 \sin(\theta_1)]^T ; \mathbf{b}_2 = [A_{2x} + \rho_2 \cos(\theta_2) \quad \rho_2 \sin(\theta_2)]^T ;$$

$$\mathbf{b}_3 = [A_{3x} + \rho_3 \cos(\theta_3) \quad A_{3y} + \rho_3 \sin(\theta_3)]^T .$$

Thus, the constraint Jacobian can be put in the following form:

$$\frac{\partial \Gamma}{\partial \boldsymbol{\theta}} = 2 \begin{bmatrix} \rho_1 (A_{2x} s_1 + \rho_2 s_{12}) & \rho_2 (\rho_1 s_{21} - A_{2x} s_2) & 0 \\ 0 & -\rho_2 ((A_{2x} - A_{3x}) s_2 - \rho_3 s_{23} + A_{3y} c_2) & \rho_3 ((A_{2x} - A_{3x}) s_3 - \rho_2 s_{23} + A_{3y} c_3) \\ \rho_1 (A_{3x} s_1 - \rho_3 s_{31} - A_{3y} c_1) & 0 & -\rho_3 (A_{3x} s_3 - \rho_1 s_{31} - A_{3y} c_3) \end{bmatrix} \quad (5)$$

where $s_i = \sin(\theta_i)$, $c_i = \cos(\theta_i)$ and $s_{ij} = \sin(\theta_i - \theta_j)$.

3. Jointspace Singular Curves

The manipulator is in a singular configuration whenever the axes of its three leg rods are concurrent or parallel¹⁷.

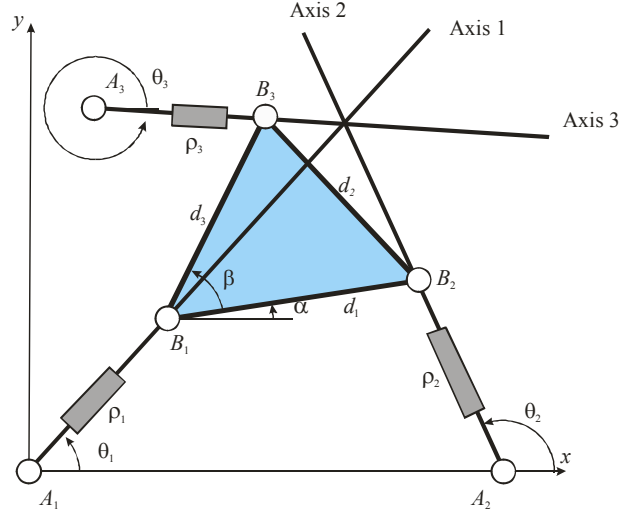


Fig 2. A 3-RPR parallel manipulator on a singular configuration

We derive the condition for the three leg axes to intersect at a common point (possibly at infinity). We first write the equations of the three leg axes:

$$\begin{cases} (\text{Axis 1}) : y \cos(\theta_1) = x \sin(\theta_1) \\ (\text{Axis 2}) : y \cos(\theta_2) = (x - A_{2x}) \sin(\theta_2) \\ (\text{Axis 3}) : y \cos(\theta_3) = (x - A_{3x}) \sin(\theta_3) + A_{3y} \cos(\theta_3) \end{cases} \quad (6)$$

Eliminating x and y in (6) yields the following singularity equation in the task parameters ($\theta_1, \theta_2, \theta_3$):

$$A_{2x}s_2s_{31} + (A_{3x}s_3 - A_{3y}c_3)s_{12} = 0 \quad (7)$$

where $s_i = \sin(\theta_i)$, $c_i = \cos(\theta_i)$ and $s_{ij} = \sin(\theta_i - \theta_j)$.

It is possible to express Eq (7) as function of the joint space parameters ρ_1, ρ_2 and ρ_3 by using the constraint equations of the 3-RPR manipulator. However, the resulting equation would be too complicated to yield real insights and difficult to handle. Our approach to compute the singular configurations in the joint space consists in reducing the dimension of the problem. We consider two-dimensional slices of the configuration space by fixing the first leg rod length ρ_1 .

Step 1: We rewrite Eq. (7) as a function of ρ_1, α and θ_1 using the constraint equations of the manipulator:

$$\begin{cases} A_{2x} + \rho_2 c_2 - \rho_1 c_1 - d_1 \cos(\alpha) = 0 \\ \rho_2 s_2 - \rho_1 s_1 - d_1 \sin(\alpha) = 0 \\ A_{3x} + \rho_3 c_3 - \rho_1 c_1 - d_3 \cos(\alpha + \beta) = 0 \\ A_{3y} + \rho_3 s_3 - \rho_1 s_1 - d_3 \sin(\alpha + \beta) = 0, \end{cases} \quad (8)$$

The first (resp. last) two equations make it possible to express ρ_2 (resp. ρ_3) as function of ρ_1 , α and θ_1 . Then, c_2 and s_2 (resp. c_3 and s_3) are calculated as function of ρ_1 , α and θ_1 from the first (resp. last) two equations of (8) and their expressions are input in Eq. (7), which, now, depend only on ρ_1 , α and θ_1 .

Step 2: We fix a value for ρ_1 , so Eq. (7) depends now only on α and θ_1 . By varying α or θ_1 , we compute the roots of the equation, to obtain the singular configurations (α_s, θ_{1s}) for a fixed ρ_{1s} .

Step 3: For every singular configuration computed in the second step of the approach, we calculate the corresponding values ρ_{2s} and ρ_{3s} using equation system (9). We have thus the singular configurations curves in a slice of the joint space (ρ_2, ρ_3) for a fixed value of ρ_1 :

$$\begin{cases} \rho_2 = \sqrt{\frac{(-A_{2x} + \rho_1 \cos(\theta_1) + d_1 \cos(\alpha))^2 + (\rho_1 \sin(\theta_1) + d_1 \sin(\alpha))^2}{}} \\ \rho_3 = \sqrt{\frac{(A_{3x} - \rho_1 \cos(\theta_1) - d_3 \cos(\alpha + \beta))^2 + (A_{3y} - \rho_1 \sin(\theta_1) - d_3 \sin(\alpha + \beta))^2}{}} \end{cases} \quad (9)$$

Figure 3 shows a slice of the joint space singular configurations for $\rho_1=17$ obtained for the same 3-RPR manipulator used by several authors^{1,8,9}, which has the following geometric parameters: $A_1 = (0, 0)$, $A_2 = (15.91, 0)$, $A_3 = (0, 10)$, $d_1 = 17.04$, $d_2 = 16.54$ and $d_3 = 20.84$ in an arbitrary length unit. We refer only to this manipulator in this paper in order to illustrate our work.

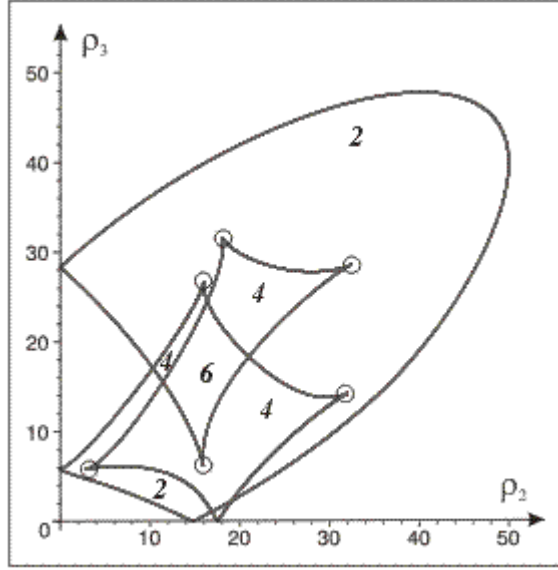


Fig 3. Singular curves in (α, θ_1) for $\rho_1=17$. Number of assembly modes is displayed in each region

Figure 3 shows the singular curves in the joint space slice (ρ_2, ρ_3) defined by $\rho_1=17$. These curves give rise to several regions with 2, 4 or 6 direct kinematic solutions. The six points pinpointed with circles are cusp points, where three direct kinematic solutions coincide.

4. Determination of the Cusp Points

4.1 Existence condition of cusp points

For serial 3-DOF manipulators, the cusp points can be determined by deriving the condition under which the inverse kinematics polynomial admits three identical roots¹³. However this approach is much more complicated when applied to the direct kinematics polynomial of 3-RPR manipulators because this polynomial is of degree 6.

An interesting alternative approach was proposed in McAree's study⁹ by writing the condition under which the manipulator loses first and second order constraints. The resulting condition for triple coalescence of assembly modes was shown to take the following form:

$$\mathbf{v}^T \left[u_1 \frac{\partial^2 \Gamma_1}{\partial \boldsymbol{\theta}^2} + u_2 \frac{\partial^2 \Gamma_2}{\partial \boldsymbol{\theta}^2} + u_3 \frac{\partial^2 \Gamma_3}{\partial \boldsymbol{\theta}^2} \right] \mathbf{v} = 0, \quad (10)$$

where \mathbf{v} is a unit vector in the right kernel of matrix $\partial \Gamma / \partial \boldsymbol{\theta}$, and u_1, u_2, u_3 are the three

components of the unit vector \mathbf{u} that spans the left kernel. Vectors \mathbf{u} and \mathbf{v} can be chosen in the set of nonzero rows and columns of the adjoint of matrix $\partial\Gamma/\partial\theta$ (i.e. the matrix of cofactors of the transpose of $\partial\Gamma/\partial\theta$), respectively.

Calculating the adjoint of $\partial\Gamma/\partial\theta$ from Eq. (5) yields:

$$\text{adj}\left(\frac{\partial\Gamma}{\partial\theta}\right) = \begin{pmatrix} k_1k_2 & -k_2k_5 & k_3k_5 \\ k_3k_4 & k_2k_6 & k_3k_6 \\ -k_1k_4 & k_4k_5 & k_1k_6 \end{pmatrix} \quad (11)$$

where

$$\begin{aligned} k_1 &= 2\rho_2((A_{3x} - A_{2x})s_2 + \rho_3s_{23} - A_{3y}c_2) & k_4 &= 2\rho_1(\rho_3s_{13} + A_{3x}s_1 - A_{3y}c_1) \\ k_2 &= -2\rho_3(\rho_1s_{13} + A_{3x}s_3 - A_{3y}c_3) & k_5 &= -2\rho_2(\rho_1s_{12} + A_{2x}s_2) \\ k_3 &= -2\rho_3((A_{3x} - A_{2x})s_3 + \rho_2s_{23} - A_{3y}c_3) & k_6 &= 2\rho_1(\rho_2s_{12} + A_{2x}s_1) \end{aligned} \quad (12)$$

Taking \mathbf{u} (resp. \mathbf{v}) as the first row (resp. column) of (11), Eq. (10) can be written as

$$(k_1k_2 \quad k_3k_4 \quad -k_1k_4) \begin{pmatrix} k_1k_2 \frac{\partial^2\Gamma_1}{\partial\theta^2} - k_2k_5 \frac{\partial^2\Gamma_2}{\partial\theta^2} + k_3k_5 \frac{\partial^2\Gamma_3}{\partial\theta^2} \\ k_3k_4 \\ -k_1k_4 \end{pmatrix} = 0 \quad (13)$$

where

$$\begin{aligned} \frac{\partial^2\Gamma_1}{\partial\theta^2} &= 2 \begin{bmatrix} \rho_1(A_{2x}c_1 + \rho_2c_{21}) & -\rho_1\rho_2c_{21} & 0 \\ -\rho_1\rho_2c_{21} & -\rho_2(A_{2x}c_2 - \rho_1c_{21}) & 0 \\ 0 & 0 & 0 \end{bmatrix} \\ \frac{\partial^2\Gamma_2}{\partial\theta^2} &= 2 \begin{bmatrix} 0 & 0 & 0 \\ 0 & -\rho_2((A_{2x} - A_{3x})c_2 - \rho_3c_{23} - A_{3y}s_2) & -\rho_2\rho_3c_{23} \\ 0 & -\rho_2\rho_3c_{23} & \rho_3((A_{2x} - A_{3x})c_3 + \rho_2c_{23} - A_{3y}s_3) \end{bmatrix} \\ \frac{\partial^2\Gamma_3}{\partial\theta^2} &= 2 \begin{bmatrix} \rho_1(A_{3x}c_1 + \rho_3c_{31} + A_{3y}s_1) & 0 & -\rho_1\rho_3c_{31} \\ 0 & 0 & 0 \\ -\rho_1\rho_3c_{31} & 0 & \rho_3(\rho_1c_{31} - A_{3x}c_3 - A_{3y}s_3) \end{bmatrix} \end{aligned} \quad (14)$$

In McAree's study⁹, Eq. (13) was not expanded. McAree⁹ noted that the expansion of this equation was too complicated to yield any real insight.

We have developed an algorithm to solve this equation for any 3-*RPR* manipulator and we have

implemented it in Maple. This algorithm detects all the cusp points inside the joint space of any 3- $R\underline{P}R$ manipulators and computes their coordinates. We present it in next section.

4.2 Algorithm for calculating cusp points

The presence of cusp points allows the 3- $R\underline{P}R$ manipulator to undertake non-singular assembly mode changing trajectories; these special trajectories can be executed by encircling a cusp point. In their study⁹, the authors stated that cusp points are pernicious and should be avoided or designed out by judicious dimensioning.

The configuration of the 3- $R\underline{P}R$ manipulator is given by six parameters: the three rod lengths (ρ_1, ρ_2, ρ_3) , and the platform position variables $(\theta_1, \theta_2, \theta_3)$. Only three of these parameters are independent. In order to reduce the dimension of the problem, McAree⁹ shows that it is possible to consider two-dimensional slices of the configuration space by fixing one of the leg rod lengths.

By doing so, the manipulator configuration can be fully defined by only two parameters. For example, for a fixed value of ρ_1 , a configuration may be fully defined by either (α, θ_1) or (ρ_2, ρ_3) . Note that in the first case, the configuration is defined in the output space by the position and the orientation of the moving platform (ρ_1 and θ_1 define the position of B_1 in the plane and α defines the orientation of the moving platform in the plane). In the second case, the configuration is defined in the joint space by the lengths of the three leg rods.

In our work, we have always taken ρ_1 as the fixed parameter. After fixing the value of ρ_1 , we first calculate the singularity curves in (ρ_2, ρ_3) , and then we compute all the cusp points of this two-dimensional slice.

4.2.1 *Algorithm*

If we consider equation (7), we notice that it is a function of $(\theta_1, \theta_2, \theta_3)$. The existence condition of cusp points (13) is a function of (ρ_1, ρ_2, ρ_3) and $(\theta_1, \theta_2, \theta_3)$. Our first goal is to establish an equation, which is a function of $(\rho_1, \alpha, \theta_1)$, and then to solve it to obtain the coordinates of the cusp points. Thus, we first derive a set of equations from the geometry of the manipulator:

$$\left\{ \begin{array}{l} \cos(\theta_2) = \frac{-A_{2x} + \rho_1 \cos(\theta_1) + d_1 \cos(\alpha)}{\rho_2} \\ \cos(\theta_3) = \frac{-A_{3x} + \rho_1 \cos(\theta_1) + d_3 \cos(\alpha + \beta)}{\rho_3} \\ \sin(\theta_2) = \frac{\rho_1 \sin(\theta_1) + d_1 \sin(\alpha)}{\rho_2} \\ \sin(\theta_3) = \frac{-A_{3y} + \rho_1 \sin(\theta_1) + d_3 \sin(\alpha + \beta)}{\rho_3} \end{array} \right. \quad (15)$$

The algorithm for detecting cusp points is implemented in MAPLE; its steps are presented below:

1. First, the expression of $\cos(\theta_2)$, $\cos(\theta_3)$, $\sin(\theta_2)$ and $\sin(\theta_3)$ in (15) are substituted into the singularity equations (7). Then, $\sin(\alpha)$ and $\cos(\alpha)$ (resp. $\cos(\theta_1)$ and $\sin(\theta_1)$) are written as function of $\tan(\alpha/2)$ (resp. of $\tan(\theta_1/2)$). As a consequence we obtain an equation of the form:

$$F_1(\rho_1, t, t_1) = 0 \quad (16)$$

where $t = \tan(\alpha)$ and $t_1 = \tan(\theta_1)$.

2. Then, the expression of $\cos(\theta_2)$, $\cos(\theta_3)$, $\sin(\theta_2)$ and $\sin(\theta_3)$ in (15) are substituted into equations (12) and (14). Applying then the tan-half substitution as above yields an equation of the form:

$$E_1(\rho_1, t, t_1) = 0 \quad (17)$$

So, we notice that the two equations (7) and (13) are written now as function of three parameters only.

3. We fix now ρ_1 , and we input the manipulator parameters $d_1, d_2, d_3, A_{2x}, A_{3x}$ and A_{3y} . We have noticed that the direct substitution of the real values of $\sin(\beta)$ and $\cos(\beta)$ into equations (16) and (17) make the equations resolution very complicated in the following steps. Thus,

we write $\sin(\beta)$ and $\cos(\beta)$ as a function of an intermediate parameter h , which is the altitude of the moving triangle.

4. The Maple *resultant* function is used to eliminate $t = \tan(\alpha)$ from the two equations (16) and (17). The resulting equation is a polynomial of degree 96 in $t_1 = \tan(\theta_1)$, which can be factored as follows:

$$P_1^{a_1} P_2^{a_2} P_3^{a_3} \dots P_{n-1}^{a_{n-1}} P_n^{a_n} Q = 0 \quad (18)$$

where Q is a 24th-order univariate polynomial in t_1 and P_1, P_2, \dots, P_n are quadratic and quartic polynomials in t_1 . Note that the factor form could not be obtained without the intermediate parameter h .

5. We input the parameter h value. We solve equation (18). Each real root t_{1i} is back-substituted into (16), which is then solved for t . For every t_{1i} , we obtain different values for t_{ij} . Finally, we get a number of solution couples (t_{ij}, t_{1i}) .
6. We substitute the values of each solution couple (t_{ij}, t_{1i}) into (17), and we keep only those solutions that satisfy this equation.

The solutions (t_{ij}, t_{1i}) kept in the last step should give the coordinates of the cusp points. To verify this, we calculate the direct kinematic solutions for each solution (t_{ij}, t_{1i}) . In many instances, we have found that some solutions do not yield three coincident solutions. This means that they are not associated with cusp points. So we reject them and we keep only those solutions that give three coincident direct kinematic solutions. These couples are the coordinates of the cusp points, we call them $(\alpha_{ij}, \theta_{1i})_{\text{cusp}}$.

After running our algorithm hundreds of times, we have noticed that in each case all cusp points were determined by the 24th-order polynomial Q of equation (18), that is, all remaining factors provided spurious solutions. Thus, we may conjecture that the cusp points are determined by Q , although we have no mathematical proof for this fact. All real roots of Q are the cusp points.

With this conjecture, our algorithm simplifies significantly because instead of solving (18) (a 96th order polynomial), we just have to solve polynomial Q (a 24th order polynomial).

To implement this result in the algorithm, we must change steps 5 and 6 into the following steps 5' and 6', and eliminate step 7:

- 5'. We input the real value of parameter h . We solve the polynomial Q . We substitute every real root θ_{i_i} of Q into equation (16), and solve it for $\tan(\alpha/2)$. For every θ_{i_i} , we obtain different values α_{ij} . Finally, we get a number of couples $(\alpha_{ij}, \theta_{i_i})$.
- 6'. We substitute the values of each couple $(\alpha_{ij}, \theta_{i_i})$ into equation (17). The couples that satisfy this equation are the coordinates of the cusp points. We call them $(\alpha_{ij}, \theta_{i_i})_{\text{cusp}}$.

Finally, to obtain the coordinates of the cusp points in the joint space (ρ_1, ρ_2, ρ_3) , we use the system of equations (9) computed from the geometry of the manipulator. We then obtain the cusp points in a slice of the joint space for a fixed value of ρ_1 .

In step 7 of the algorithm, we have noticed that the existence condition of cusps generates solutions that do not provide triple direct kinematic solutions. This confirms the statement of McAree⁹ that the cusp existence condition that he established is a sufficient condition but not a necessary one.

4.2.2 *Algorithm Execution*

The algorithm execution time slightly depends on the value of ρ_1 and of the 3-*RPR* manipulator parameters. It highly depends on the number of digits required for the calculation. For 90 digits (which is necessary to guaranty a good accuracy), it is about two minutes on a computer equipped with a 3GHz-Pentium 4 with 512 Mo of Ram.

We present the results of an execution of the algorithm, for the same 3-*RPR* parallel manipulator introduced in section 3. For the same fixed value $\rho_1=14.98$, as the one used in previous papers^{8,9}, the algorithm detects six cusp points instead of five identified in the paper⁹. Figure 4 shows the singular curves of the 3-*RPR* manipulator for $\rho_1=14.98$, and the six cusp points

pinpointed with circles. The sixth point missed by McAree⁹ is the point A, it is circled with bold lines and in-boxed in a separate view. The zoomed view shows that it is really a cusp point.

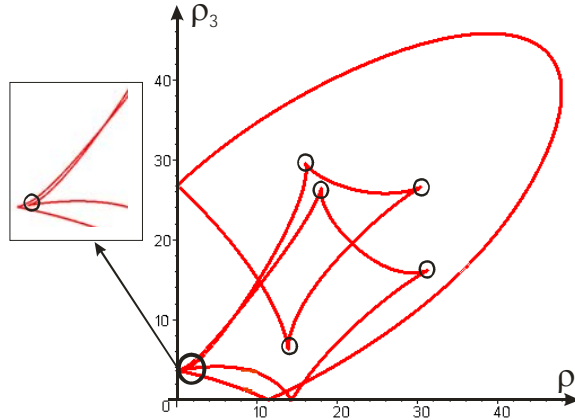


Fig 4. Singular curves and cusp points in a slice of the 3-RPR manipulator joint space (ρ_2, ρ_3) for $\rho_1=14.98$.

The coordinates of the six cusp points are given in the table 1 below

	α	θ_1	ρ_2	ρ_3
Cusp A	50.67 deg	-69.12 deg	0.84	3.77
Cusp B	-2.59 deg	177.32 deg	13.85	6.26
Cusp C	-122.89 deg	114.05 deg	31.27	16.17
Cusp D	57.48 deg	133.77 deg	30.44	26.61
Cusp E	-0.59 deg	15.46 deg	16.02	29.56
Cusp F	170.37 deg	-10.65 deg	17.98	26.44

Tab 1. Coordinates of the six cusp points for $\rho_1=14.98$.

5. Descriptive Analysis

In this section, the singular curves are analysed in several slices of the joint space for the manipulator studied in papers^{8,9} and whose geometric parameters were given in section 3. Figure 5 depicts the singular curves for increasing values of ρ_1 and shows that the number of cusp points is not the same for all slices as we may have 0, 2, 4, 6 or 8 cusp points. In Fig. 5, regions with two assembly modes (resp. four, six) are filled in light grey (resp. in dark grey, in black). Zero-cusp slices are obtained for very small values of ρ_1 only ($\rho_1=0.05$ in Fig. 5), where the singular curves are made of two separate closed curves that define only one small region with two assembly modes and a large void (note, the two curves are so close that the region cannot be seen in Fig. 5). When ρ_1 is

increased, two cusp points appear, the void gets smaller and a four-solution region appears ($\rho_1=2$). Then two more cusp points appear, defining one more four-solution region ($\rho_1=2.8$). We have six cusp points and a small void at $\rho_1=6$; for $\rho_1=8, 10, 12, 14, 16, 18, 20, 24$ and 26 , we have always six cusp points but the void is replaced with a six-solution region. Eight cusp points exist in a small vicinity of $\rho_1=27$. Then two cusp points and the six-solution region disappear ($\rho_1=29$). Finally, the number of cusp points stabilizes to four, defining one central four-solution region surrounded by a two-solution region ($\rho_1=31, \dots$). Interestingly, this last pattern is very similar to the one often observed in a cross-section of the workspace of 3-*R* serial manipulators¹⁹. However, serial manipulators feature the same pattern in all cross-sections (the sections which passes through the first revolute joint axis), and variation in the number of cusp points arises only from a modification of the manipulator geometry.

The above analysis shows that the joint space topology of 3-*RPR* manipulators is very complicated. Contrary to serial manipulators, the shape of the singular curves and the number of cusps points depend on which slice is chosen in the joint space. Thus, planning trajectories is not easy. However, we have noticed that the pattern stabilizes for sufficiently large values of ρ_1 .

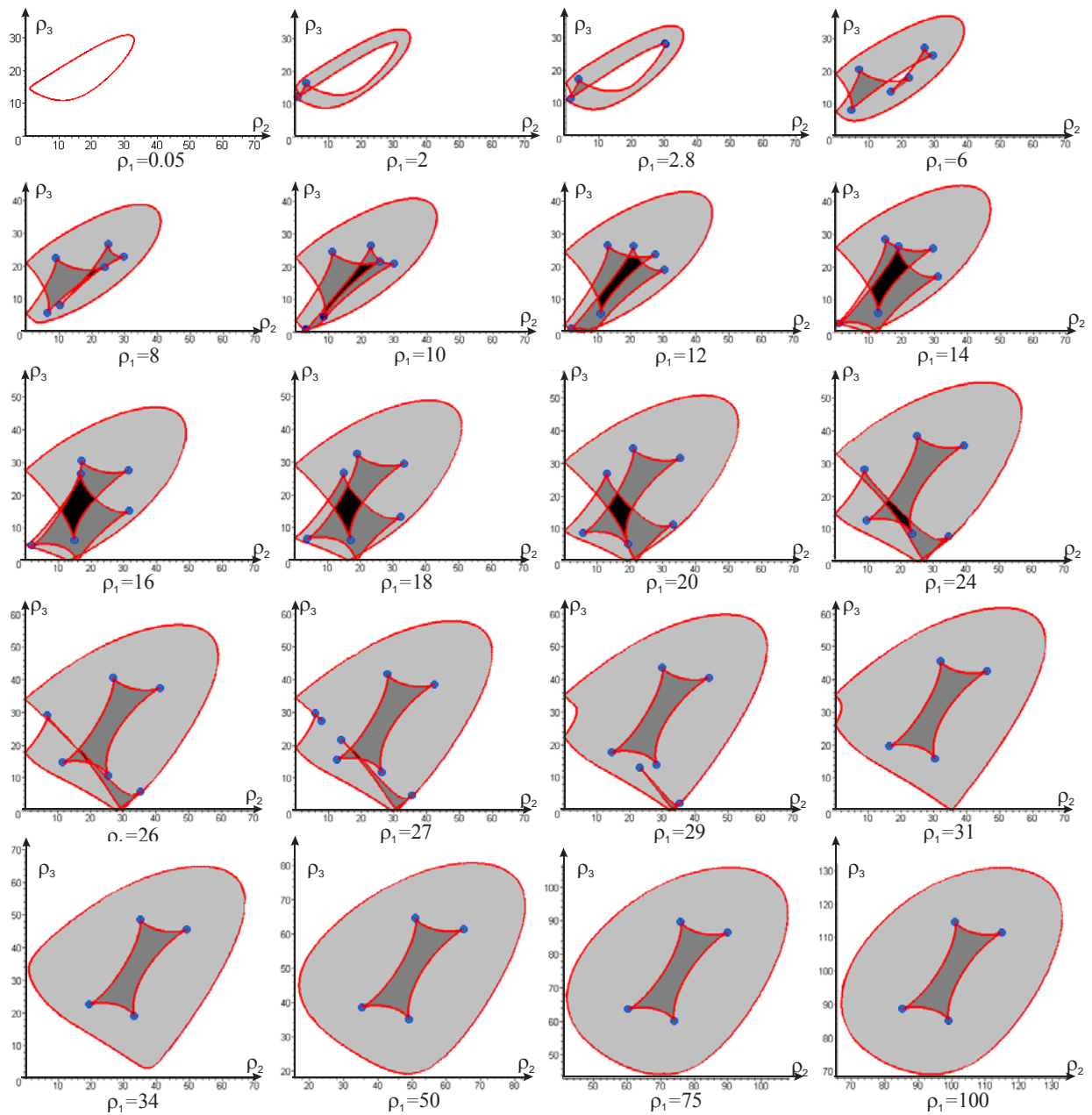


Fig 5. Singular curve patterns for increasing values of ρ_1 .

Figure 6 represents the singularities in the joint space of the manipulator studied when ρ_1 varies from 0 to 50. To obtain this surface, we have imported the solutions obtained in step 4 into a CAD software, and we have meshed them together.

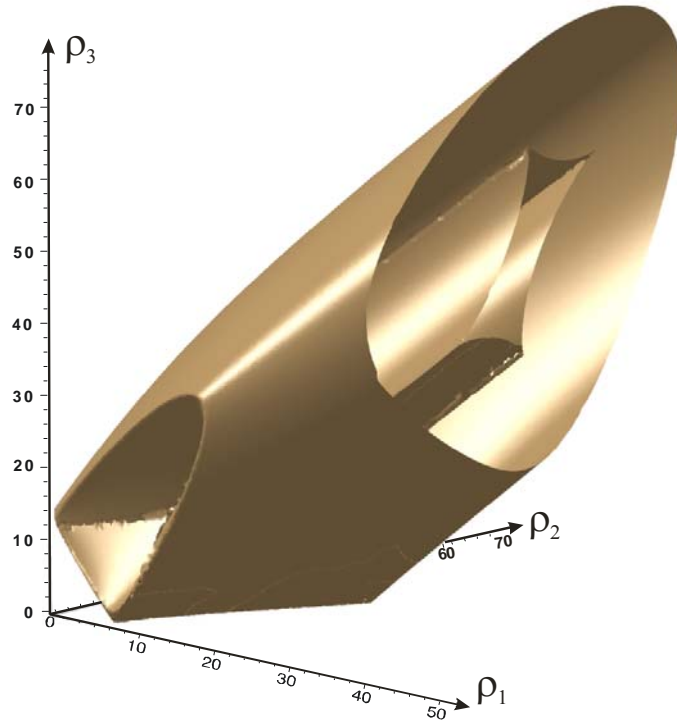


Fig 6. Joint space singularity surfaces of the 3-RPR manipulator studied when ρ_1 varies from 0 to 50.

The surface depicted in Figure 6 is of interest:

i. for planning trajectories in the joint space because it shows clearly the joint space regions that are free of singularities.

ii. for manipulator design, because it offers a tool for defining the values of the joint limits such that the joint space is a singularity-free box.

We can see clearly in figure 6 how the number of cusp points and the topology of the slices stabilize for $\rho_1 > 31$.

This feature has been observed in many other manipulator geometries. For example, the 3-RPR manipulator defined by the following geometric parameters: $A_1 = (0,0)$, $A_2 = (3,0)$, $A_3 = (1.1,2.7)$, $d_1 = 1.3$, $d_2 = 0.9$ and $d_3 = 0.4$ in an arbitrary length unit, has a constant pattern as soon as $\rho_1 > 5$ (Fig. 7). Note that, in contrast with the stabilized pattern obtained for the preceding manipulator, this pattern features a large void.

Most of the research work on parallel manipulators has focused on the analysis and optimization of the workspace. If the workspace is useful for manipulator design, the analysis of

singular curve patterns in the joint space can be used as a complementary tool to compare several manipulator geometries.

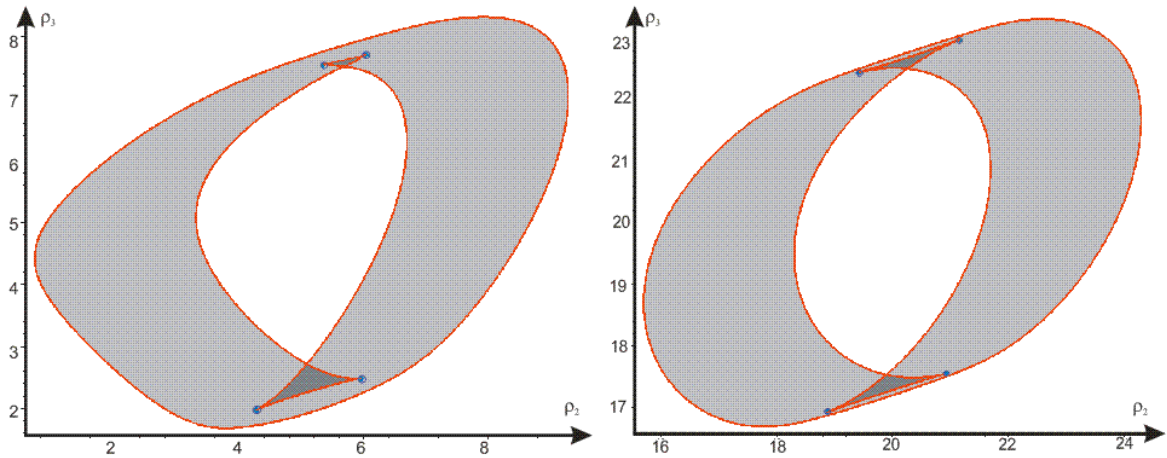


Fig 7. Stabilized singular curve patterns for another manipulator geometry plotted for $\rho_1=5$ (left) and $\rho_1=20$ (right).

6. Conclusions

A procedure for computing joint space singularities of $3-R\underline{P}R$ parallel manipulators has been presented in this paper. Then, the existence condition of cusp points defined by McAree⁹ has been reviewed and exploited. An algorithm able to detect and to compute cusp points inside any section of the joint space of any $3-R\underline{P}R$ parallel manipulator has been established. To the best of the authors' knowledge, such an algorithm had never been proposed before. The algorithm results in a 96th degree univariate polynomial that can be put in a factored form. We have showed with intensive numerical experiments that the coordinates of the cusp points are the real roots of a 24th degree univariate polynomial, which is one of the factors of the 96th polynomial. Finally, a descriptive analysis of the singular curves in slices of the joint space of $3-R\underline{P}R$ parallel manipulators has been conducted, with a special focus on the cusp points on these singular curves. It has been shown that, contrary to what arises in serial manipulators where any cross section of the workspace exhibits the same pattern of singular curves and cusp points, this pattern depends on the choice of the slice in the joint space for a given $3-R\underline{P}R$ parallel manipulator. On the other hand, we have noticed that it is possible to have a constant pattern by adjusting the joint limits. It has been observed that the

maximum number of cusps depends on the manipulator geometry . No manipulators were found with more than eight cusp points. Most of the research work on parallel manipulators has been focused on the analysis and optimization of the workspace. This paper provides a complementary tool that helps better understand the topology of the joint space of parallel manipulators and finds applications in both design and trajectory planning.

7. References

1. J-P. Merlet, *Parallel Robots*, Kluwer Academics, 2000.
2. C. Gosselin, and J. Angeles, "Singularity analysis of closed loop kinematic chains," *IEEE Transactions on Robotics and Automation*, vol. 6, no. 3, 1990.
3. C. Gosselin, J. Sefrioui, and M.J. Richard, "Solution polynomiale au problème de la cinématique directe des manipulateurs parallèles plans à 3 degrés de liberté," *Mechanism and Machine Theory*, vol. 27, no. 2, pp. 107-119, 1992.
4. J. Sefrioui, and C. Gosselin, "On the quadratic nature of the singularity curves of planar three-degree-of-freedom parallel manipulators," *Mechanism and Machine Theory*, vol. 30, no. 4, pp. 535-551, 1995.
5. P. Wenger, and D. Chablat, "Definition sets for the direct kinematics of parallel manipulators," *8th Conference on Advanced Robotics*, pp. 859-864, 1997.
6. I. Bonev, D. Zlatanov, and C. Gosselin, "Singularity Analysis of 3-DOF Planar Parallel Mechanisms via Screw Theory," *ASME Journal of Mechanical Design*, vol. 125, no. 3, pp. 573–581, 2003.
7. K.H. Hunt, and E.J.F. Primrose, "Assembly configurations of some In-parallel-actuated manipulators," *Mechanism and Machine Theory*, vol. 28, no. 1, pp.31-42, 1993.
8. C. Innocenti, and V. Parenti-Castelli, "Singularity-free evolution from one configuration to another in serial and fully-parallel manipulators. *Journal of Mechanical design*. 120. 1998.
9. P.R. McAree, and R.W. Daniel, "An explanation of never-special assembly changing motions for 3-3 parallel manipulators," *The International Journal of Robotics Research*, vol. 18, no. 6, pp. 556-574. 1999.
10. Xianwen Kong and Clément M. Gosselin, "Forward displacement analysis of third-class analytic 3-RPR planar parallel manipulators," *Mechanism and Machine Theory*, Vol. 36, No. 9, pp. 1009--1018.

11. J. W. Burdick, "A Classification of 3R regional manipulator Singularities and Geometries," In *Proceeding IEEE International Conference on Robotics and Automation*, pp. 2670-2675, Sacramento, California, 1991.
12. Ph. Wenger, "A New General Formalism for the Kinematic Analysis for all Non-Redundant Manipulators," In *Proceeding International Conference on Robotics and automation*, pp. 442-447, Nice, France, 1992
13. J. El Omri and P. Wenger, "How to recognize simply a non-singular posture changing 3-DOF manipulator," *Proc. 7th Int. Conf. on Advanced Robotics*, p. 215-222, 1995.
14. E. Ottaviano, M. Husty and M. Ceccarelli, "A cartesian representation for the boundary workspace of 3R manipulators," In *Proc. On Advances on Robots Kinematics*, p. 247-254, 2004.
15. Ph. Wenger and D. Chablat, "Workspace and Assembly modes in Fully-Parallel Manipulators : A Descriptive Study," *Advances in Robot Kinematics and Computational Geometry*, Kluwer Academic Publishers, pp. 117-126, 1998.
16. M. Zein, Ph. Wenger and D. Chablat, "Singular curves and cusp points in the joint space of 3-RPR parallel manipulators", *Proceedings of the 2006 IEEE International Conference on Robotics and Automation*, Orlando, Florida, May 2006.
17. K. H. Hunt, "Geometry of Mechanisms," *Clarendon Press*, Oxford, 1978.
18. B. Buchberger, G. E Collins and R. Loos: "Computer Algebra: Symbolic & Algebraic Computation," *Springer-Verlag*, Wien, pp. 115-138, 1982.
19. M. Baili, P. Wenger and D. Chablat, "A classification of 3R orthogonal manipulators by the topology of their workspace," *IEEE Int. Conf. on Robotics and Automation*, Louisiana, USA 2004.